ADVANCED HEALTHCARE MATERIALS
www.advhealthmat.de

Repurposing Nano-Dimensions of a Small Phytomolecule, Rhein, Into Nano-Rhein to Unveil Its Efficacy on Hypercalciuria-Induced Nephropathies on a SERS-Based Calcification Profiling Platform

*Madhukrishnan Murali, Vishnu Priya Murali, Roopasree O Jayarajan, Abeesh P, Daisy R Sherin, Jayadev S Arya, M M Vishnu Prasad, Elambalassery G. Jayasree, Lekha K Nair, Sreejith P Panicker, and Kaustabh Kumar Maiti**

Renal disorders induced by calcium oxalate (CaOx) crystals potentiate a complex pathophysiological landscape devoid of effective pharmacological interventions. Herein, a bioactive herbal compound, rhein, isolated from *Cassia fistula Linn* is known for its well-documented anti-inflammatory and anti-cancer properties. It's role as a CaOx inhibitor has received inadequate scrutiny. The clinical viability of rhein is hampered bypoor aqueous solubility and low bioavailability. To surmount these challenges, a simple and rapid sonochemical self-assembly technique is engineered to transform rhein into nano-rhein, aiming to augment its inhibitory efficacy toward CaOx. The anti-calcification properties of both rhein and nano-rhein were assessed through an in vitro model employing human embryonic kidney cells HEK-293. Through surface-enhanced Raman scattering (SERS), we established a Raman imaging platform to monitor calcification processes. To deepen the understanding of cellular responses to CaOx we conducted an RNA sequencing experiment to evaluate the the transcriptomic modification exerted by nano-rhein. In addition, in vivo studies further demonstrated that nano-rhein significantly reduced renal CaOx crystal deposition and alleviated kidney injury and dysfunction in a C57BL/6 mouse model. This exploration offers intricate insights into the potential of rhein, particularly in its nano form, as a promising therapeutic agent for CaOx-induced nephropathies.

1. Introduction

Renal disorders induced by calcium oxalate (CaOx) crystals are a prominent etiological contributor to various kidney pathologies, including oxalate nephropathy (ON), particularly in individuals grappling with chronic kidney disease (CKD), end-stage renal disease (ERSD), and metabolic disorders.[1] CKD represents a pathological state characterized by a gradual and progressive decline in renal function over time.[2] This degeneration results in the accumulation of waste products and excess fluids within the body, giving rise to various systemic complications. Among these complications is the emergence of CaOx crystals in the kidney tubules, a condition identified as ON.[3] Hyperoxaluria, characterized by an excessive oxalate excretion in the urine, often underlies the pathogenesis of ON.[4] The surplus oxalate in the urine binds with calcium, forming kidney stones and crystals, thereby contributing to the development of ON. The recurrence of kidney stones and crystals

M. Murali, V. Priya Murali, R. O Jayarajan, A. P, J. S Arya, M M V. Prasad, K. Kumar Maiti
Chemical Sciences & Technology Division (CSTD) & Bioscience and Bioengineering Division (BBD)
CSIR-National Institute for Interdisciplinary Science & Technology (CSIR-NIIST)
Industrial Estate, Pappanamcode, Thiruvananthapuram, Kerala 695019, India
E-mail: kkmaiti@niist.res.in
M. Murali, R. O Jayarajan, J. S Arya, K. Kumar Maiti
Academy of Scientific and Innovative Research (AcSIR)
Ghaziabad 201002, India

V. Priya Murali
Amala Integrated Medical Research Department (AIMRD)
Amala Institute of Medical Sciences
Amala Nagar, Thrissur 680 555, India
D. R Sherin
Kerala Digital University Technocity Campus
Mangalapuram, Thonnakkal PO 695317, India
E. G. Jayasree
Department of Applied Chemistry
Cochin University – CUSAT
Kalamassery, Kochi, Kerala 682022, India
L. K Nair
Department of Pathology
Amala Institute of Medical Sciences
Amala Nagar, Thrissur 680555, India
S. P Panicker
Department of Zoology
University of Kerala
Thiruvananthapuram 695 581, India

The ORCID identification number(s) for the author(s) of this article can be found under https://doi.org/10.1002/adhm.202504133

DOI: 10.1002/adhm.202504133

can inflict considerable damage on the kidneys, potentially culminating in kidney failure.[5] In the context of CKD, the systemic levels of oxalate surge due to the kidneys serving as the primary route of oxalate excretion. A diminished Glomerular Filtration Rate (GFR) results in heightened concentrations of oxalate in plasma and glomerular ultrafiltrate, exposing the remaining tubular cells to increased oxalate concentrations. This exposure can prompt the formation of oxalate clumps or crystals, further exacerbating renal damage as these calcium oxalate crystals traverse through the renal system.[6] Despite available treatments aimed at symptom management and slowing CKD progression, a definitive cure for the disease remains elusive. Consequently, there is a pressing need for research into innovative therapeutic strategies for CKD. Current therapeutic interventions under consideration encompass a spectrum of approaches, including the use of phosphate binders, vitamin K, sodium thiosulphate, Myoinositol hexaphosphate (IP6), bisphosphonates, TNAP inhibitors, and Denosumab.[7]

Top of Form, However, currently, there is no effective treatment to reduce or reverse calcifications. Nevertheless, some treatments can decelerate calcification's progression, such as phosphate binders, bisphosphonates, active vitamin D, sodium thiosulphate, and cinacalcet.[1] Reports indicate that hydroxycitrate, when ingested orally, is excreted via urine, positioning it as a promising therapeutic agent for stone treatment.[8–10] Biomacromolecules, particularly polysaccharides enriched with acidic polyanionic groups, have been identified as potent inhibitors of CaOx calculus formation.[11] Rhein, a lipophilic anthraquinone characterized as 4,5-dihydroxyanthraquinone-2-carboxylic acid, is abundantly present in various medicinal herbs.[12] The biological activities of Rhein, particularly those pertinent to human health, are currently under active investigation.

Accumulating evidence indicates that Rhein exhibits a plethora of pharmacological properties, encompassing hepatoprotective, nephroprotective, anti-inflammatory, antioxidant, anticancer, and antimicrobial activities.[12–14] It has demonstrated inhibitory effects on a variety of cancers, including but not limited to, breast, cervical, colon, lung, and ovarian cancers, under both in vitro and in vivo conditions.[15–17] Recent research has shed light on the ability of this compound to modulate diverse signaling pathways within cancer cells, thereby inhibiting angiogenesis and impeding the progression of various cancer types.[15–17] Despite the therapeutic potential of rhein, its clinical application is significantly limited due to its poor aqueous solubility and low bioavailability, which is primarily attributed to the metabolism of glucuronidation in the liver.[13] To overcome these limitations and enhance the therapeutic efficacy of Rhein, several strategies have been exploited, including the development of polymeric microparticles and nanoparticles encapsulating Rhein.[14,18] However, these approaches often encounter challenges such as drug loss during the fabrication process and premature release of the payload, leading to lower drug loading and potential systemic toxicity.[14,18,19] We propose that a promising solution to these challenges could be the directed self-assembly of Rhein, into a nanoparticle form with the help of probe sonication, which may offer enhanced therapeutic efficacy.

In the present investigation, Rhein, an active compound isolated from *Cassia fistula* Linn. (CF), was found to self-assemble into nanoparticles through intermolecular π-π interactions and hydrogen bonding (**Scheme 1**). Notably, these Rhein nanoparticles, which we named as Nano-Rhein (NR) exhibited superior anti-calcification properties compared to Rhein in its free form while maintaining minimal cytotoxicity.

To elucidate the mechanisms underlying this enhanced CaOx inhibitor activity, we conducted a comprehensive exploration that included in vitro anti-calcification assays using Alizarin Red S staining in HEK-293 cells, the establishment of a robust Raman imaging platform with a SERS-based Alizarin Red S assay for profiling CaOx inhibitors, and comprehensive RNA sequencing followed by Reactome pathway analysis to understand transcriptomic modifications and the mitigating effects of rhein/nano-rhein. of the molecular processes involved. Our findings indicate that the nanoparticle of Rhein is a much better candidate for CaOx inhibition than its molecular form of the compound. These characteristics position Rhein nanoparticles as a promising therapeutic agent for the treatment of nephrocalcinosis. Furthermore, in vivo study in a C57BL/6 mouse model of calcium oxalate-induced nephrocalcinosis demonstrated that nano-rhein significantly reduced renal CaOx crystal deposition, prevented renal injury, and improved kidney function, showcasing its superior efficacy compared to both free rhein and the standard citrate. Further studies are warranted to fully understand the potential of these nanoparticles in clinical applications. As per our knowledge, it is the first time to report the CaOx inhibitory effects of Rhein and its nano form.

2. Results and Discussion

2.1. Synthesis and Morphological Characterization of Nano-Rhein (NR)

We have isolated the rhein from ethanol extract of CF seeds and flowers (Figures S1, S2, Supporting Information). Anti-urolithiasis assessment conducted at both the extract and compound levels, utilizing Alizarin Red S (ARS) assays, has demonstrated the potent anti-calcification properties of the ethanolic extract of CF and the compound rhein (Figure S9, Supporting Information). In this work, we have utilized the sonochemical self-assembly of rhein molecule for enhanced inhibition of CaOx crystals (**Figure 1**a). Rhein NPs (NR) were characterized by UV, IR, TEM, SEM, and AFM, respectively (Figure 1b–f). Its morphology was found to be belt-like structure. The TEM analysis after 30 days, indicates the superior stability of NR at room temperature (Figure S16, Supporting Information). In addition, the self-assembled NPs maintained colloidal stability in 50% FBS (fetal bovine serum) for up to 6 hours with the SEM analysis (Figure S7, Supporting Information). Although no surfactants or excipients were applied, the NR displayed desirable stability without any precipitation and phase separation.

2.2. The Self-Assembly Mechanism of Rhein Nanoparticles

The structure of rhein aggregates was examined using DFT calculations. All the calculations are performed using the Gaussian 09 suite of programs employing Minnesotta hybrid density functional M06-2x at the 6–311+G(d,p) basis set. The stable structure of the rhein dimeric form has been calculated, resembling

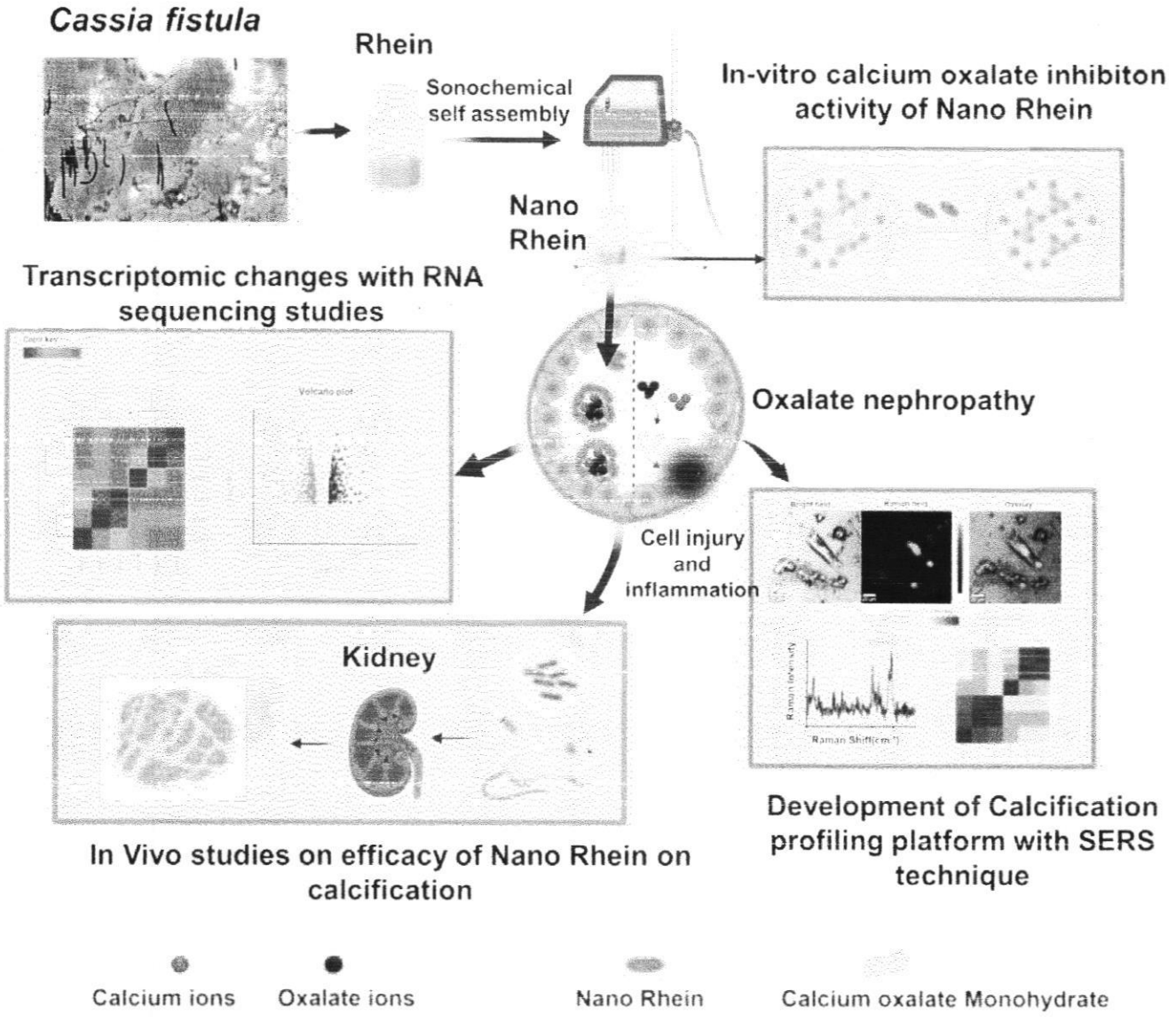

Scheme 1. Isolation of rhein and synthesis of nanorhein, in vitro calcium oxalate inhibition activity of nanorhein using Alizarin Red S assay, Development of calcification profiling platform using SERS technique, mechanistic evaluation of the in vitro decalcification effect nanorhein through of RNA sequencing and transcriptomics analysis and in vivo anti-calcification studies.

it's stacking interactions (Figure 1g, h). Dimeric form with carboxyl functionalities lying in a trans manner is the most stable form over the cis (by 2.06 kcal mol^{-1}) or the ones with inter monomeric hydrogen bonds. This particular geometry was also found to have more stabilization energy due to dimer formation (-23.48 kcal mol^{-1}) (Figure S6, Supporting Information). The monomers are stacked by a distance of 3.23 Å in the trans and 3.18 Å in cis conformer. From the perfect stacking arrangement, the central ring of one monomer is found to be displaced by an angle of 22° to the next. This slipping is slightly more in the case of the cis conformer, while it is reduced to 20° in the H-bonded conformer. The aim of the analysis is to quantify the stacking interactions. The electron density and the laplacian of electron density calculated for the bond critical points between the monomers lie in the range specified for weak noncovalent interactions.[30] All the C-C bond critical points calculated between the monomers had their electron density lying in the range 0.0075-0.0085 au (trans), 0.0074–0.0084 au (cis), and the Laplacian of electron density lying in the range 0.025–0.026 au (trans), 0.021–0.025 au (cis) (Figure 1g, h). This observation was further substantiated by subsequent HRMS analysis (Figure S5, Supporting Information). The HRMS analysis revealed the presence of monomers (m/z 283.0249), and dimers (m/z 589.0388) while higher-order aggregates were not detected. These aggregates were observed to exist as sodium salt clusters. Notably, the dimers were the most prevalent aggregate ions, suggesting a relative stability of the dimer configuration compared to other aggregates.

This evidence substantiates that the building blocks of rhein nanoparticles are indeed rhein monomers and the sodium salt of rhein. To further elucidate the self-assembly mechanism of

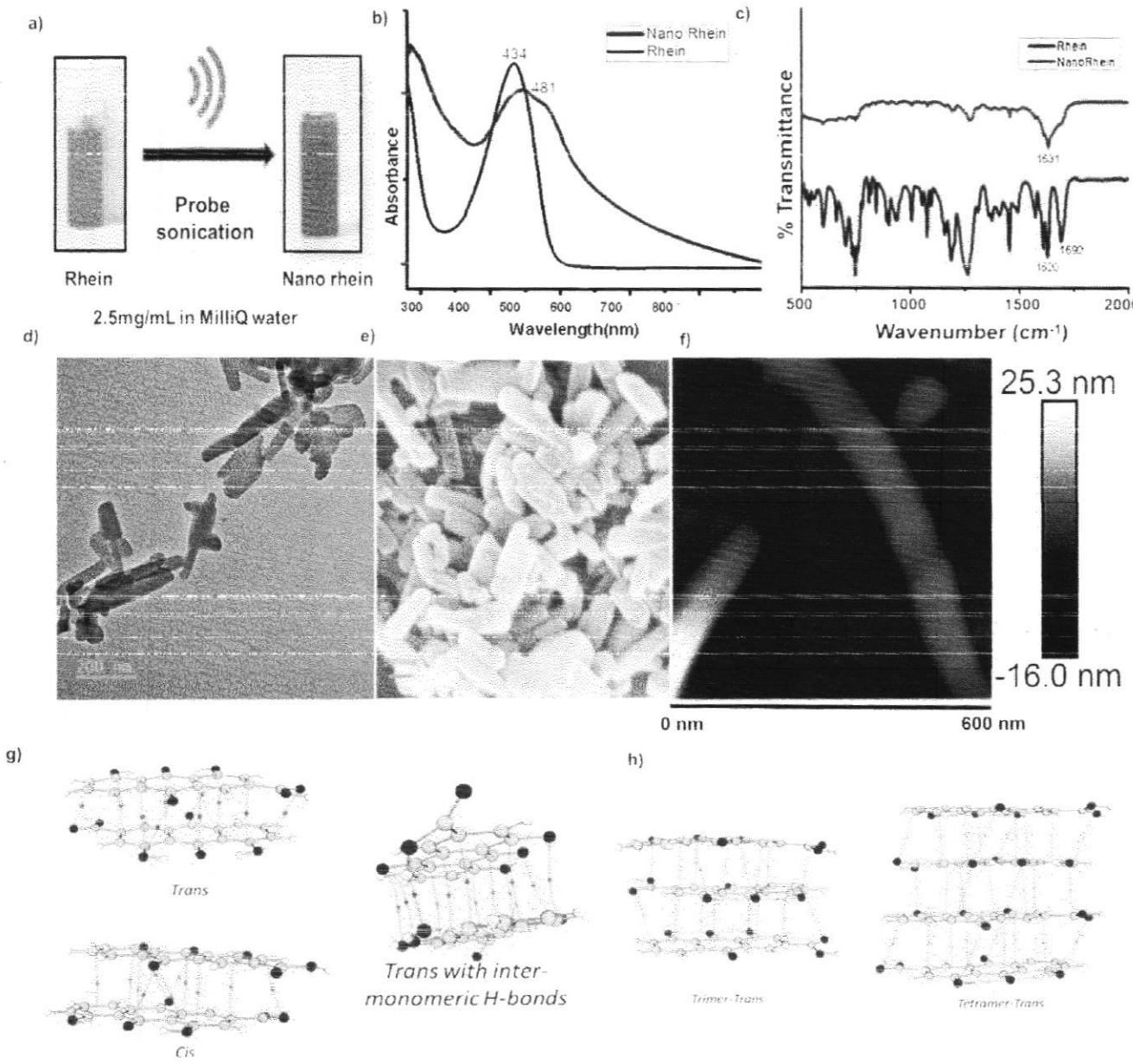

Figure 1. a) Synthetic procedure of Nano Rhein b) UV–vis spectrum of Rhein and Nano Rhein showing shift in the wavelength c) IR spectrum of Rhein and Nano rhein showing shift in the carbonyl group d) TEM e) SEM and f) AFM images of Nano Rhein. g) The geometry and stability of rhein dimers are assessed by DFT calculations h) DFT calculations of higher oligomers – trimer and tetramer.

Nano-rhein (NR), we conducted additional spectroscopy studies (Figure 1b, c).

Analysis of the FT-IR results revealed a characteristic absorption peak for the C = O peak at 1692 cm^{-1} shifted to 1631 cm^{-1}. These alterations suggest the participation of hydrogen bonds in the self-assembly process.[20] The observed maximum red-shift was associated with the existence of the anthraquinone excimer, primarily influencing the self-assembly process through π-π interactions.[20] The results obtained from the X-ray diffraction (XRD) analysis provided further substantiation for our findings. A prominent peak was observed at a d-spacing value of 3.4 Å. This peak is indicative of the characteristic intermolecular distance associated with π-π stacking interactions between the two molecules (Figure S15, Supporting Information). Notably, in UV-visible spectrum, the peak underwent a bathochromic shift from 434 nm to 481 nm during the preparation of Nano rhein via the probe sonication method (Figure 1b). This shift can be attributed to the π-π interactions inherent to the anthraquinone structure.[20] Furthermore, this observation suggests a transformation in the aggregate configuration from H-type to J-type aggregation, which is indicative of changes in the molecular arrangement and packing within the Nano rhein structure.[20] Emission spectrum of Nano Rhein showing an additional shoulder peak to that of the Rhein confirming the changes in the

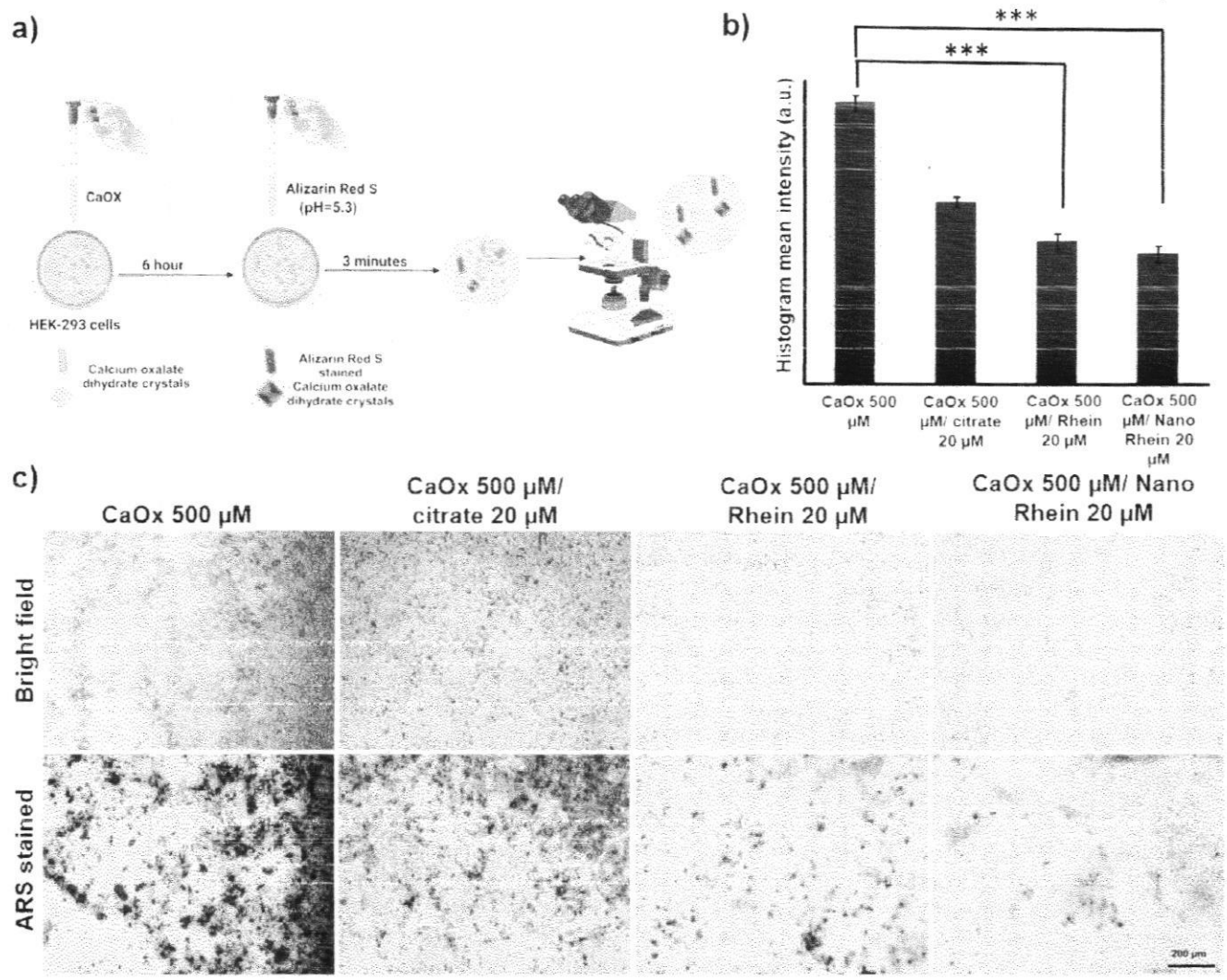

Figure 2. a) Schematic representation of Alizarin Red S assay, b) quantified bar diagram of Alizarin red S imaging assay using image J software. One-way ANOVA followed by a Tukey-Kramer multiple comparison test were performed. (***) $p < 0.001$ as compared with CaOx 500 µM/Rhein 20 µM (CaOx 500 µM versus CaOx 500 µM/Rhein 20 µM) and (***) $p < 0.001$ as compared with CaOx 500 µM/Nano Rhein 20 µM (CaOx 500 µM versus CaOx 500 µM/Nano Rhein 20 µM). Data are presented as mean ± SD (n = 3). c) Top row showing bright field images of CaOxCaOx 500 µM, CaOxCaOx 500 µM/Rhein 20 µM CaOxCaOx 500 µM/Nano Rhein 20 µM while bottom row showing stained images of CaOxCaOx 500 µM, CaOxCaOx 500 µM/Rhein 20 µM and CaOxCaOx 500 µM/Nano Rhein 20 µM. Magnification 100X, Scale bar 200 µm.

structural arrangement of Nano Rhein to that of the Rhein (Figure S17, Supporting Information).

2.3. Nano Rhein and Its Enhanced Anti- Calcification Property Compared to Rhein

Ethanol extracts derived from the flower and seed components of CF were found to be the most effective in ARS staining experiments (Figure S8, Supporting Information). The alizarin red S assay is considered the gold standard for the quantification of calcium mineralization and is thus widely used among the scientific community.[21] Five compounds were isolated from these ethanol extracts, with the anthraquinone rhein being the most active one in the in vitro anti-urolithiatic studies. In this study conducted at the compound level, rhein demonstrated superior activity compared to other compounds and even outperformed the positive control, citrate. (**Figure** 2a–c; Figure S9, Supporting Information).

The cytotoxic potential of the investigated compounds was quantitatively assessed via the 3-(4,5-dimethylthiazol-2-yl)-2,5-diphenyltetrazolium bromide (MTT) assay. The administration of both rhein nanoparticles and the rhein molecule was observed to exhibit negligible cytotoxic effects on the human embryonic kidney cells HEK-293. This observation was consistent across a concentration range of 20–50 µM, with the assessment conducted at the 24-hour mark post-administration. The lack of significant cytotoxicity suggests that these compounds, within the specified concentration range, maintain the viability of HEK-293 cells (Figure S3, Supporting Information). Upon administration of the rhein compound at a concentration of 75 µM, a significant reduction in the viability of HEK-293 cells

was observed, with a decrease of 29% compared to the rhein nanoparticles. Intriguingly, the viability of HEK-293 cells remained unaffected across various concentrations when treated with rhein nanoparticles. These findings indicate that the cytotoxicity exhibited by rhein nanoparticles is notably lower than that of the rhein molecule. The biocompatibility of NR with varying concentrations of 10 μM to 200 μM was also assessed with Hemolysis assay Figure 4; Figure S4 (Supporting Information). This suggests that the transformation of rhein into nanoparticles could be a promising strategy for reducing its cytotoxic effects on HEK-293 cells, thereby potentially enhancing its therapeutic index.

2.4. Mechanism of CaOx Inhibition by Nanorhein

From the literature, it is obvious that carboxylate (COO−) groups present in NR may have the ability to coordinate with Ca^{2+} ions, and hydrogen bonding interactions can be established between the hydroxyl (OH) groups in NR and the carboxylate ions in the oxalate groups of amorphous calcium-oxalate nanoparticles.[9,22] To elucidate the mechanism of CaOx inhibition by Nanorhein, a Scanning Electron Microscopy (SEM) analysis was conducted. (**Figure** 3a–g).

In a 12-well plate, $CaCl_2$ and $Na_2C_2O_4$ (NaOx) were added in situ to achieve a final concentration of 1 mM each. This was accomplished by diluting a 50 mM stock solution of each compound with Phosphate-Buffered Saline (PBS, pH = 6.2). The formation of calcium oxalate dihydrate (COD) type crystals was observed in the control and early incubation stages of CaOx and Nanorhein. However, as the incubation time increased, the crystal size began to shrink, transitioning from an octahedral shape to a linear one. This suggests that the addition of Nanorhein significantly inhibited the bulk crystallization of CaOx (Figure 3a–c).

In addition, we observed the growth that was specific to the face of the crystal. This could be due to the inhibitor's tendency to bind preferentially to a particular face of the crystal, which is determined by its unique molecular surface arrangement. This phenomenon was demonstrated by the transformation of COD crystals into a needle-like shape as the concentrations of NR's increased (**Figure** 4d–g). This was also confirmed with the Raman spectral analysis and TGA experiments where the NR-treated CaOx showed different patterns in both the Raman spectrum and TGA curves (Figure S8, Supporting Information).

DFT studies showed that the preferable deprotonation at the carboxyl sites and the stabilization of the resulting anion by intramolecular hydrogen bonding would facilitate its salt formation with cations. The energy of formation for the calcium salt of deprotonated cis- rhein dimer from its anionic monomer is computed to be -440.29 kcal mol^{-1}. This value is comparable to the energy of the formation of stable calcium oxalate from its ions (-514.53 kcal mol^{-1}) (Figure 3h). Also, we performed the NO assay to confirm the enhanced efficacy of NR towards calcification as nitric oxide regulates calcification by interfering with TGF- signaling (Figure 3i). On treatment with the CaOx of 500 μM NO concentration was seen to be increased which was reduced on the simultaneous treatment of CaOx 500 μM/ rhein 50 μM and CaOx 500 μM/ nano rhein 50 μM.

2.5. Cellular Uptake of Rhein and Nanorhein on HEK-293 Cells

The internalization of rhein and nanorhein in HEK-293 cells was investigated to gain a deeper understanding of their distinct mechanisms, particularly regarding their anti-calcification efficacy and cellular interactions.

Studies on cellular internalization in the absence of CaOx crystals highlighted significant kinetic differences between the two treatments (Figure 4b). Rhein demonstrated relatively rapid cellular internalization, which was largely complete by approximately 6 hours.

Nanorhein, however, exhibited a markedly different and slower cellular uptake profile. Its internalization commenced around 6 hours and was complete by approximately 24 hours (Figure 4b). This slower uptake of nanorhein suggests a potential for sustained intracellular release of rhein from the nanocarriers. This characteristic could contribute to more durable protective effects and influence cellular responses at later time points. The overall enhanced therapeutic efficacy of nanorhein likely arises from this combination of potent extracellular activity against CaOx crystals and a modified, sustained intracellular delivery profile. Further investigation into the intracellular fate of rhein using colocalization studies with organelle-specific markers provided insights into its subcellular distribution. Confocal laser scanning microscopy (CLSM) images showed that internalized rhein (R) exhibited substantial colocalization with MitoTracker Green (MG), a mitochondrial marker. The Pearson's Correlation Coefficient (PCC) for rhein and MitoTracker Green was 0.80, indicating a significant degree of colocalization with mitochondria). In contrast, colocalization with Hoechst (H), a nuclear stain, was minimal, with a PCC of 0.008 (Figure 4a).

Confocal fluorescence microscopy revealed different interactions of rhein and nanorhein with calcium oxalate (CaOx) crystals when co-incubated with HEK-293 cells for 3 hours. Nanorhein (NR 50 + CaOx 1 mM) primarily interacted directly with CaOx crystals on the cell exterior (Figure 4c). This is likely due to its larger particulate nature. In contrast, rhein (R 50 + CaOx 1 mM) at the same concentration was predominantly internalized into the cells within the same timeframe (Figure 4c). This suggests that nanorhein's enhanced ability to inhibit CaOx crystallization and protect renal cells from crystal-induced injury might stem from its strong, immediate extracellular activity against the crystals.

2.6. SERS Platform for Monitoring Calcification Processes

In this study, we utilized surface-enhanced Raman spectroscopy (SERS), an ultrasensitive analytical technique that intensifies the Raman scattering phenomenon of molecules adsorbed onto through nanostructures or coarse nanometallic surfaces.[23] This method enables the rapid detection of chemical species with high sensitivity and molecular-level specificity.[24] Despite the potential of SERS in various applications, its use in in vitro calcification image profiling platforms for analyzing CaOx inhibitors has been scarcely reported.

For the first time, we present a SERS imaging platform for profiling CaOx inhibitors and various calcification processes (**Figure** 5a). We developed a SERS-based ARS assay, wherein

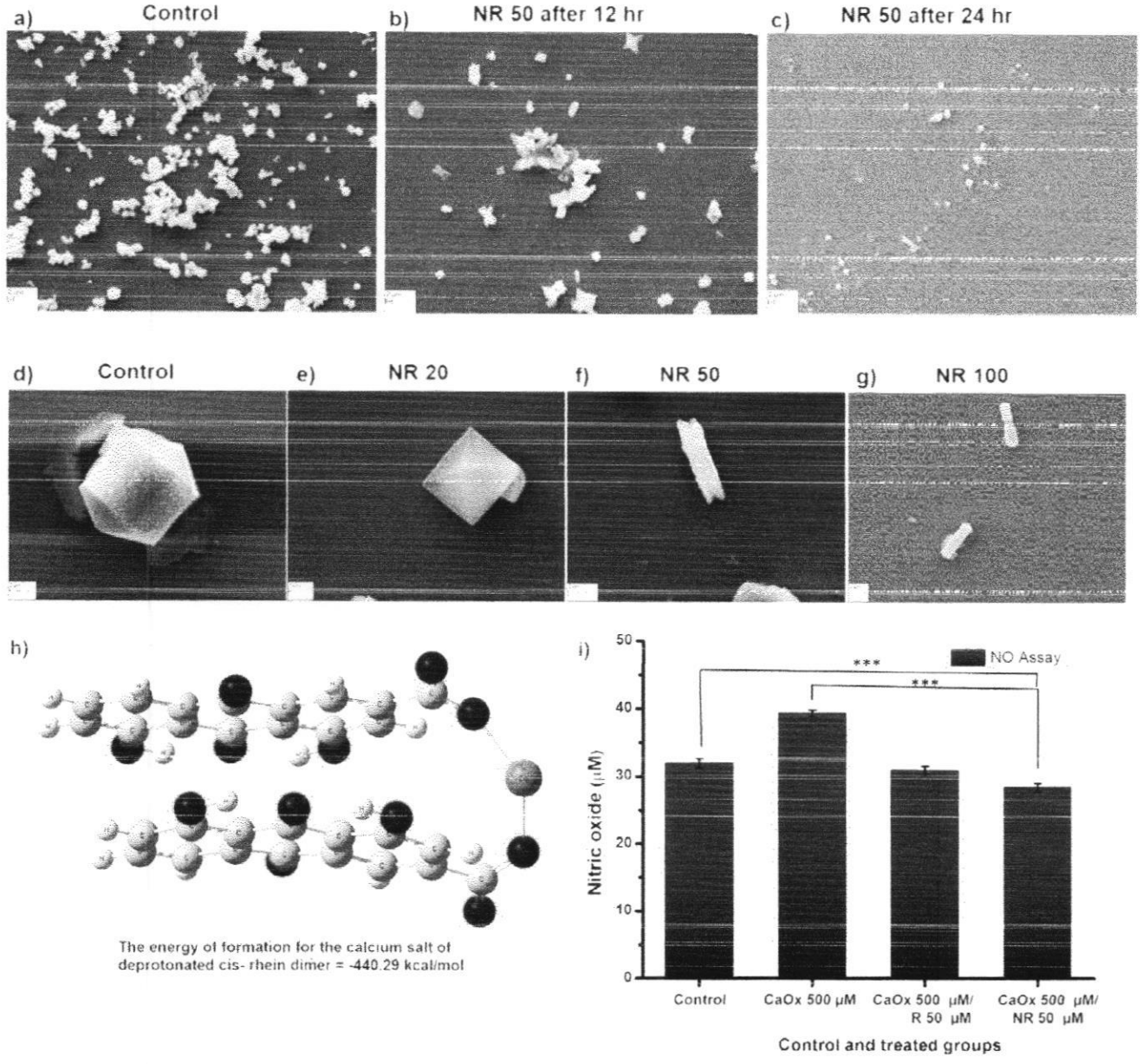

Figure 3. Mechanism of CaOx inhibition by Nano rhein- SEM images of a–c) Reduction of CaOx crystals on treatment with the NanoRhein, CaOx 500 μM as control, CaOx 500 μM/Nano rhein 50 μM 12hr, CaOxCaOx 500 μM/Nano Rhein 50 μM 24 hr d–g) Conversion of COM crystals to COD and needle-like crystals on treatment with the CaOxCaOx 500 μM as control, CaOxCaOx 500 μM/Nano rhein 20 μM 24 hr, CaOxCaOx 500 μM/Nano rhein 50 μM 24 hr, CaOx CaOx500 μM/Nano rhein 100 μM 24 hr h) Energy optimized structure of Ca salt of Rein Dimer (cis) i) NO assay of HEK-293 cells in plain medium taken as control, CaOxx 500 μM, rhein 50 μM, Nano rhein 50 μM for 24 h incubation. Graphical representation showing the NO levels for all the treatments. Data are presented as mean ± SD (n = 3). One-way ANOVA followed by a Tukey-Kramer multiple comparison test were performed. (***) $p < 0.001$ as compared with control group (Control versus CaOx 500 μM/NR 50 μM) and (***) $p < 0.001$ as compared with CaOx 500 μM (CaOx 500 μM versus CaOx 500 μM/NR 50 μM).

varying concentrations of CaOx crystals were crystallized by incubating Calcium Chloride ($CaCl_2$) and Sodium Oxalate (NaOx) for 24 hours in a 6-well plate seeded with cells. Concurrently, rhein and Nanorhein were administered along with CaOx. Subsequently, the medium was removed from the plate, washed thrice with Phosphate-Buffered Saline (PBS), and incubated with ARS (pH = 5.3) for 3 minutes for staining the CaOx crystals. The plate was then washed thrice again with PBS, incubated with 40 nm gold nanoparticles (AuNP) for five minutes and subjected to SERS imaging. ARS dye at pH 5.3 with the addition of 10% ammonium hydroxide seems to be giving much better SERS intensity than the normal ARS solution when incubated with the AuNP (Figures S11, S12, Supporting Information). This may be due to the deprotonation processes of the two hydroxylic groups that occur at higher pH.[47] This prompted us to design the SERS-based ARS assay. Our results indicated that as the

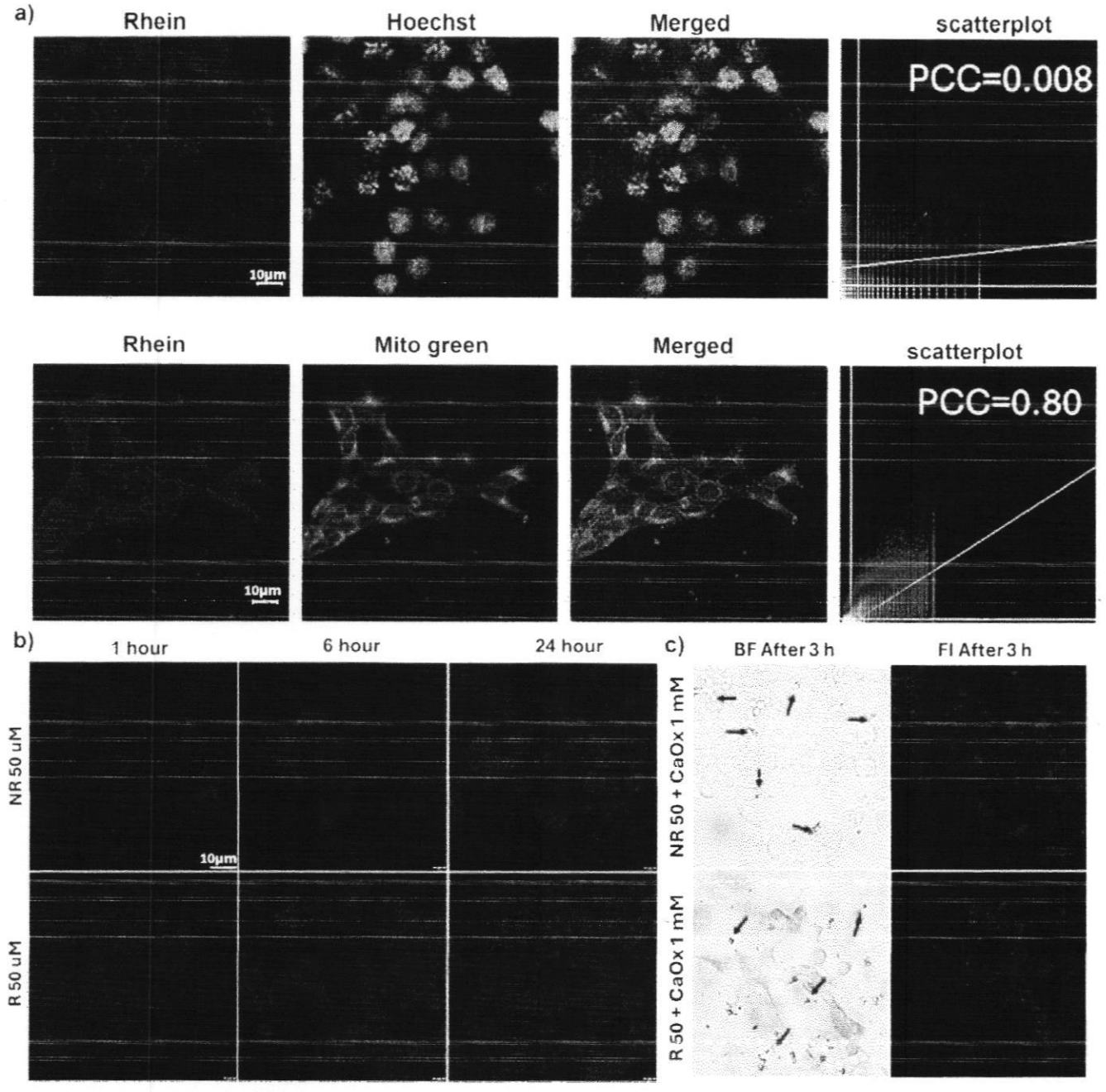

Figure 4. Cellular internalisation of rhein and Nanorhein. a) CLSM images showing the colocalisation of rhein in mitochondria b) Cellular internalisation of rhein and Nanorhein of 50 μM at different time points c) CLSM images showing preferential binding of Nanorhein toward CaOx crystals in comparison with the rhein (arrow points the CaOx crystals; Rhein/Nanorhein treatment concentration, 50 μM, CaOx – 1 mM). Scale bar – 10 μm.

concentration of CaOx increased, the SERS intensity of ARS also increased (Figure 5c). With this assay, we were successfully able to image and analyze the SERS intensities of stained ARS upto 10 μM of CaOx. The SERS intensities have been demonstrated as heatmaps for each concentration of CaOx as well as for the CaOx treated with inhibitors to understand the effect of inhibitor on CaOx crystallization (Figure 5d). Interestingly, the crystallization on cells treated with 50 μM nanorhein resulted in a lower SERS intensity compared to its CaOx counterpart (500 μM), thereby demonstrating its superior anti-nephrolithiasis capability compared to the positive control, citrate (Figure 5c; Figure S9, Supporting Information). By successfully identifying CaOx inhibitors using this SERS-based ARS assay, this technique could pave the way for the development of new therapeutic strategies for CaOx-induced nephropathies and other related disorders. It could also contribute to the broader field of nanomedicine by providing a powerful tool for the study of biological processes at the molecular level as the technique possesses high sensitivity compare

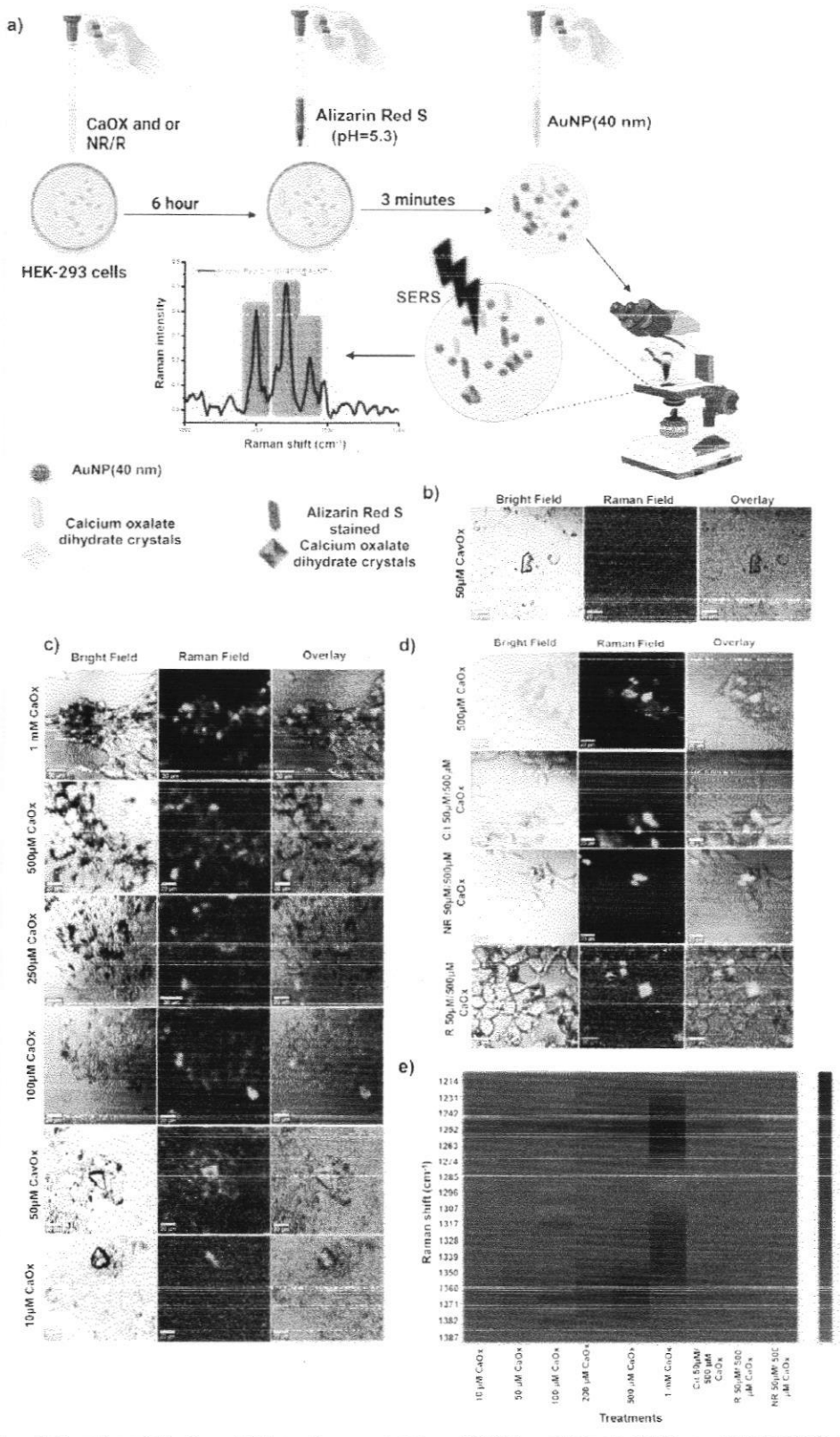

Figure 5. SERS imaging platform for calcification. a) Schematic representation of SERS-based Alizarin Red S assay b) bright field, Raman field and overlay images of AunP treated cells incubated only with CaOx 50 μM without the addition of Alizarin Red S c) its SERS images of various concentrations of CaOx as well as d) CaOx 500 μM, NR 50 μM / CaOx 500 μM, Cit 50 μM / CaOx 500 μM, and R 50 μM / CaOx 500 μM e) its SERS intensities represented as Heatmap. Scale bar – 20 μM.

to the original staining protocol and it represents a non-invasive modality.

A key advantage of our SERS approach, is its superior sensitivity compared to conventional ARS staining by microscopy, particularly for detecting low levels of calcification. While conventional ARS staining by microscopy can visually confirm the presence of calcification, our SERS-Alizarin Red S (ARS) assay demonstrates the capability to detect calcium oxalate down to 10 micromolar concentrations. This level of sensitivity is often challenging to achieve with standard ARS assays without sophisticated signal amplification strategies and may allow for the detection of earlier or more subtle stages of calcification. Furthermore, the intensity of the SERS signal can be directly correlated with the concentration of the analyte or the extent of its binding. While fluorescence intensity can also be quantitative, SERS offers a robust platform for quantification, especially at the low detection limits we have achieved. This high specificity and photostability further complement visual imaging techniques by providing quantifiable data even at early calcification stages.

In addition the upregulation of cell surface markers during calcium crystallization and their expression levels during the anti-urolithic activity of rhein were investigated. It is well-established that these cell surface markers are upregulated during calcification as a defensive mechanism against calcium crystals.[25–27] In our previous work, the compound GlcNPhAlk was utilized as a cell surface glycan marker to differentiate glycan expression in cancerous and normal cells.[28,29] In the current study, metabolic glycan labelling of the GlcNPhAlk molecule was employed to understand glycan expression during the calcification process. Interestingly, increased labeling of cell surface glycans was observed as calcification progressed, indicating an upregulation of cell surface glycan upon calcium crystallization. However, when the NR was administered alongside CaOx, glycan expression gradually declined (Figure S10a—c, Supporting Information). This suggests a potential role for nanorhein in modulating glycan expression during calcification.

2.7. CaOx-Induced Transcriptomic Changes Reflect Oxalate Nephropathic Processes In Vitro and Were Prevented by Nano Rhein

To further understand the cellular response to CaOx and to interpret the associated cellular changes, we performed an RNA sequencing experiment. Cells were cultured as in the ARS imaging assay and treated with 500 µM CaOx spiked medium (positive ctrl), 500 µM CaOx spiked medium premixed with 50 µM NR, medium only (negative ctrl). Hierarchical clustering of differentially expressed genes between positive and negative control showed a drastic change in gene expression profile with CaOx treatment, which was prevented by NR spiking (**Figure** 6a). In ctrl versus CaOx samples, 137 differentially expressed genes with a fold change ≥ 0.5 and $p \leq 0.05$ were detected, similarly CaOx versus CaOx/NR and Control versus CaOx/NR samples contain 1112 and 887 differentially expressed genes, respectively; (Figure 6b).

Based on these findings and the established roles of inflammation and fibrosis in CaOx nephropathies,[34,35] our analysis focused on key DEGs. In our subsequent analysis, we investigated the expression levels of individual genes, with a specific focus on distinct gene groups. These included immune response pathways, particularly those associated with inflammatory responses, as well as extracellular matrix (ECM) proteins and cell cycle and proliferation processes. Our data confirmed that CaOx crystals induce a significant pro-inflammatory and pro-calcific transcriptomic shift, hallmarked by the elevated expression of TNF receptor superfamily members (*TNFRSF12A, TNFRSF13C*), *TNFAIP3*, and the interleukin-6 receptor (*IL6R*) (**Figure** 7c, d). The activation of *TNFRSF12A* (TWEAKR) is particularly noteworthy, as it is a known promoter of inflammation and osteogenic differentiation in renal cells.[36] The altered expression of *TNFAIP3* (A20) suggests a dysregulated inflammatory state, as it is a critical negative regulator of NF-κB signaling.[37] This inflammatory cascade is compounded by the upregulation of *INHBA*, a member of the TGF-β superfamily whose product, Activin A, is a potent pro-fibrotic factor in the kidney that can drive an osteogenic phenotype.[38,39] Concurrently, the marked upregulation of the *FOS* gene family (*FOS, FOSB, FOSL1, FOSL2*) reflects a robust cellular stress response, as these proteins form the AP-1 transcription factor, a master regulator of cell proliferation, differentiation, and inflammation during renal injury.[40,41]

In stark contrast, the intervention with nano-rhein demonstrated a potent ability to counteract these pathological transcriptomic changes, which aligns with its documented anti-inflammatory properties.[42] We postulate that nano-rhein's primary protective mechanism is the significant attenuation of the initial inflammatory signaling cascade, a hypothesis supported by its known ability to inhibit the NF-κB pathway.[43,44] This is strongly evidenced in our data by the observed downregulation of *TNFRSF* members and *IL6R* in the NR-treated group. By mitigating this upstream inflammation, nano-rhein consequently suppresses the downstream activation of cellular stress markers, as shown by the normalized expression of the *FOS* gene family (Figure 6c). This is strongly evidenced in our data by the observed downregulation of *TNFRSF* members and *IL6R* in the NR-treated group. By mitigating this upstream inflammation, nano-rhein consequently suppresses the downstream activation of cellular stress markers, as shown by the normalized expression of the *FOS* gene family (Figure 6c).[31,32] The FOS gene family contains 4 members: FOS, FOSB, FOSL1, and FOSL2. The FOS proteins have been implicated as regulators of cell proliferation, differentiation, and transformation which were also upregulated on CaOx crystallization and subsequently downregulated on treatment with the NR.[33] To summarize, these results suggest that by reducing cell crystal interactions NR treatment can largely prevent CaOx-induced downstream responses, such as inflammatory signaling pathways as shown in the FPKM ratio of selected genes, especially genes like INHBA, FOS, FOSL1, FOSB, COL7A1, TNFRFS12A, and IL6R (Figure 6c).

Thus, the drastic change induced by CaOx treatment and its prevention by NR were confirmed. Reactome pathway analysis confirmed that CaOx treatment enriched pathways related to broad cellular stress and injury responses, NGF-stimulated transcription, nuclear events (kinase and transcription factor activation), by receptor tyrosine kinases (NTRKs, RTKs) (Figure 6d, Table S1, Supporting Information).

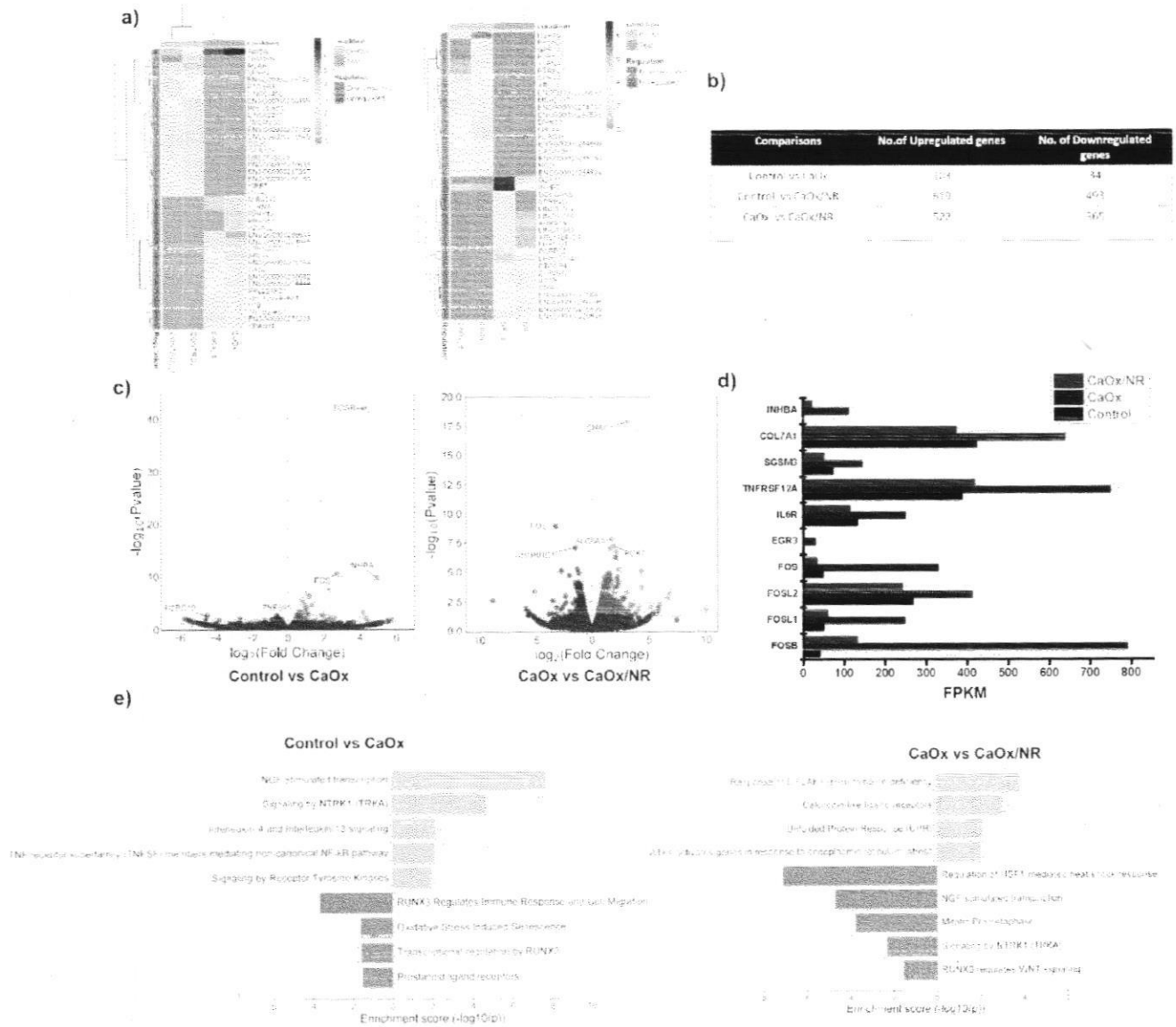

Figure 6. a) Heatmap and hierarchical clustering of relative gene expression levels determined by RNA sequencing. Top 20 differentially expressed genes between control versus CaOx, and CaOx versus CaOx / NR with $p < 0.05$, log2ratio = 0.5, and respective expression levels in the other treatment groups are plotted (red—relatively upregulated, blue—relatively downregulated). b) Table showing number of upregulated and down regulated genes in all three groupings c) Volcanoplots of differentially expressed genes between control versus CaOx, control versus CaOx/NR, and CaOx versus CaOx / NR with $p < 0.05$, log2ratio = 0.5, and respective expression levels in the other treatment groups are plotted (red—downregulated, green—upregulated) and d) Normalized count of gene transcripts (FPKM – fragments per kilobase of exon model per million reads mapped) involved in inflammatory responses, ECM composition, cell proliferation, and tissue homeostasis of the different treatment groups is plotted e) Reactome analysis of control versus CaOx, and CaOx versus CaOx / NR with $p < 0.05$.

2.8. Hypercalciuria Induced Nephropathic Processes In Vivo and Were Prevented by Nano Rhein

Building on the promising in vitro results of nano rhein, we undertook an in vivo proof-of-concept study using a mouse model of calcium oxalate (CaOx)-induced nephrocalcinosis.[22,45] Crystallization was triggered by intraperitoneal (ip) administration of glyoxalate (Gly) (75 mg k^{-1}g) daily for 7 days following previously established methods.[45,46]

C57BL/6 mice were administered with nanorhein [at doses of 10 mg k^{-1}g (Nano rhein lower dose -NRLD) and 20 mg k^{-1}g (Nanorhein Higher Dose -NRHD)], rhein ((R), 20 mg Kg^{-1}), and citrate ((Cit), 100 mg Kg^{-1}) via i.p. injection along with Gly (i.p.) once daily for seven days prior to sacrifice. Animals fed a normal diet and injected with phosphate buffered saline (i.p., 100 µL) served as the vehicle control group (VC), while those receiving the Gly (i.p.) without treatment served as the negative control (NC).

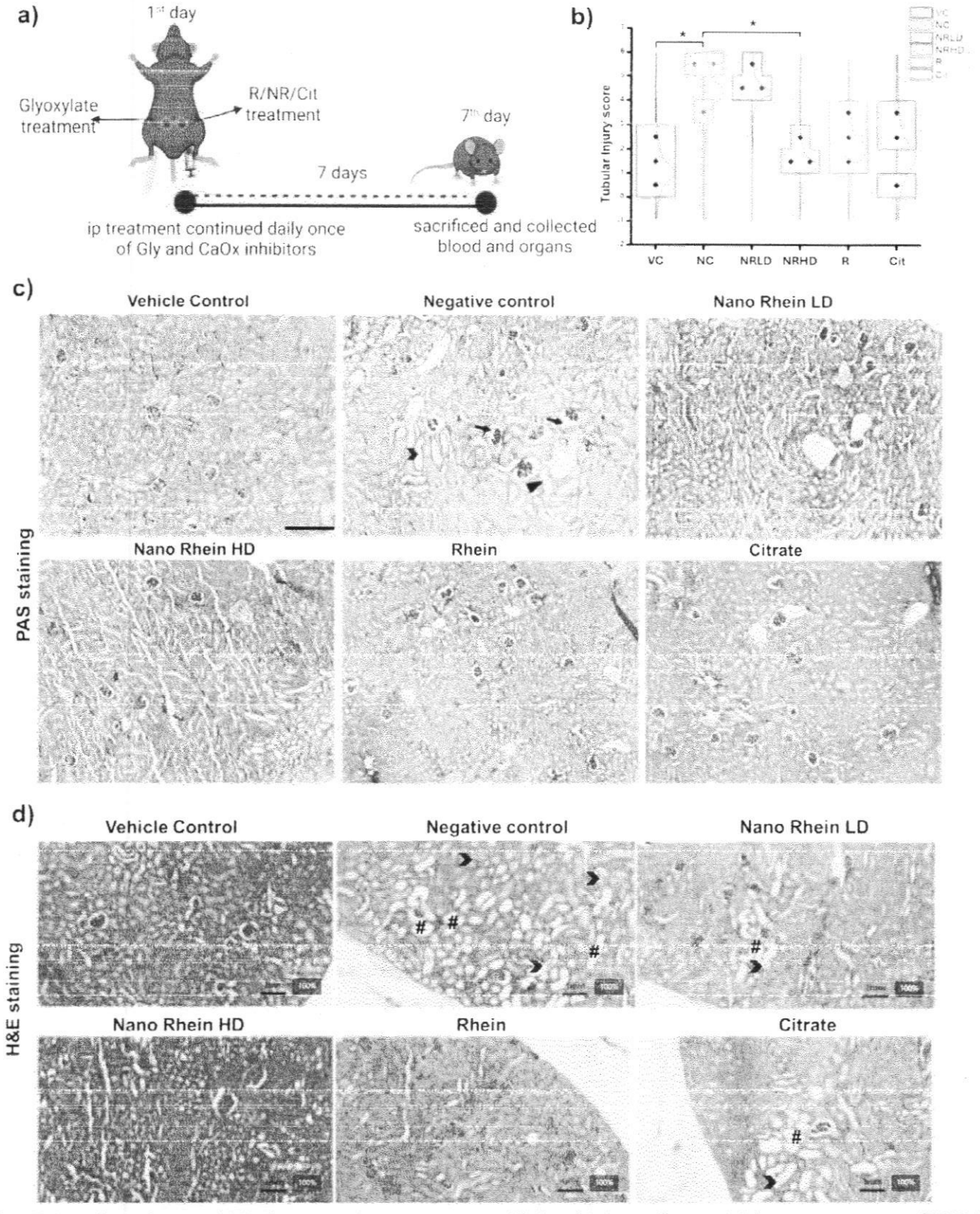

Figure 7. Nano rhein reduces renal CaOx deposition and injury in a mouse model of renal CaOx crystallization. a) Schematic representation of C57BL/6 mice treated by intra peritoneal injection of Gly (75 mg kg^{-1}) to induce renal CaOx crystallization and concurrently treated with indicated concentrations of NR/R/Cit intra peritoneally daily for seven consecutive days) b) tubular injury score of different treatment group by PAS staining. Data are presented as mean ± SD (n = 3). One-way ANOVA followed by a Tukey-Kramer multiple comparison test were performed. (*) $p < 0.05$ as compared with VC group (VC

The kidney sections were meticulously stained with Pizzolato staining to visualise CaOx deposits, revealing a remarkable dose-dependent reduction in renal CaOx levels with nanorhein and rhein, alongside citrate as the standard treatment. This significant reduction was evident across all treatment groups in comparison with the vehicle control group (Figures 7a,d, 8a,b).

Further histological analysis using Hematoxylin and Eosin (H&E) staining provided a clearer picture of the structural damage to the kidney tissue (Figure 7d). In the negative control group, kidneys exhibited severe renal injury characterized by numerous tubular casts and widespread dilated tubules, as highlighted in the images (Figure 7d). While some of this damage was still apparent in the NRLD and citrate-treated groups, the NRHD and R groups showed a marked prevention of these pathological features. The protective effect was most pronounced in the NRHD group, where the kidney sections showed minimal damage.

Further compelling evidence came from the periodic acid-Schiff (PAS) staining of kidney sections, which showcased a dose-dependent reduction in kidney injury as indicated by the scoring of tubular damage (Figure 7b,c). Moreover, plasma measurements of blood urea nitrogen and creatinine level pointed to enhanced excretory kidney function with nanorhein treatment NRHD surpassing the results from the other treatment groups (**Figure** 8c,d).

These findings suggest that nanorhein may successfully delay both crystallization and growth, while simultaneously shielding against harmful CaOx-cell interactions. Notably, no significant changes in animal weight or signs of compound toxicity were observed, reinforcing the safety profile of the treatment (Figure S14 and Table S2, Supporting Information).

3. Conclusion

In summary, we initially isolated the compound rhein from *Cassia fistula* Linn., a plant known for its medicinal properties. Despite rhein's recognized anti-inflammatory and anti-cancer activities, its potential as an anti-urolithiasis agent remains unexplored. The therapeutic application of rhein is restricted due to its poor solubility and low bioavailability. To address these limitations, we developed a simplest nano formulation of rhein, aiming to enhance its bioavailability and thereby its anti-urolithiatic activity. The efficacy of both rhein and its nano formulation in inhibiting calcification was confirmed via Alizarin Red S staining in an in vitro system using HEK-293 cells. Additionally, by harnessing the imaging capabilities of SERS, we've developed the SERS platform for monitoring calcification processes. SERS-based Alizarin Red S assay, for the purpose of profiling CaOx inhibitors and integration of a metabolic labelling technique with a surface-enhanced Raman scattering (SERS) facilitated the discernment of alterations in cell surface glycan expression during calcification and subsequent decalcification following Rhein/Nano-Rhein treatment. To further elucidate the cellular response to calcium oxalate (CaOx) and interpret the associated morphological changes observed through cellular imaging, we conducted an RNA sequencing experiment. Finally, the transcriptomic alterations induced by CaOx treatment and the preventive effect of Nano-rhein were confirmed through RNA sequencing and subsequent Reactome pathway analysis.

Importantly, in vivo studies demonstrated that, nano-rhein significantly prevented renal injury and hypercalciuria-induced nephropathy in a mouse model of calcium oxalate (CaOx)-induced nephrocalcinosis. Nano-rhein, especially at higher doses, remarkably reduced renal CaOx crystal formation and mitigated severe renal damage, outperforming both free rhein and the standard drug citrate. This structural protection translated to a significant improvement in kidney function, with nano-rhein being the most effective in reducing plasma BUN and creatinine levels. Importantly, nano-rhein showed no signs of toxicity, reinforcing its safety profile.

4. Experimental Section

All the chemicals and solvents used in this study were procured from Sigma Aldrich, Alfa Aesar, TCI, and Merck, and were used as received without any additional purification. The ^{1}H-NMR, ^{13}C spectra were obtained using a Bruker Avance 500 MHz NMR spectrometer, with chemical shifts reported in parts per million (ppm). Mass spectra were acquired under ESI/HRMS at a resolution of 61800 using a Thermo scientific exactive mass spectrometer. The absorption spectra were recorded on a Shimadzu (UV-2450) UV-Vis. spectrophotometer, and the resulting data was analyzed using Microsoft Excel and OriginPro 8.5. SERS measurements were conducted using a WITec Raman microscope (WITec Inc. Germany, alpha 300R), which employed a laser beam directed at the sample through a 20x objective and a Peltier cooled CCD detector.

The samples were excited with a 633 nm wavelength laser, and the Stokes shifted Raman spectra were collected in the range of 250 to 3000 cm^{-1} with a resolution of 1 cm^{-1}. Before each measurement, the system was calibrated using a silicon standard with a Raman peak centered at 520cm^{-1}. The WITec Project plus (v 5.2) software package was utilized for data evaluation. TEM measurements were carried out using a JEOL 2010 instrument with an accelerating voltage of 200 KV. The sample for TEM was prepared by placing a drop of the aqueous nanoparticle solution onto a 230 mesh copper grid coated with carbon, and allowing it to air dry prior to measurement.

Synthesis of Nanorhein: Nanorhein was synthesized using the probe sonication method (SKL-1200D, 120 W) by sonicating the 2.5 mg mL^{-1} solution of Rhein in milliQ water for 10 minutes. Then it was differentially centrifuged at different rpm to collect Nanorhein with a size of less than 1 µm.

DFT Studies: All the calculations were done using Gaussian 09 suite of programs employing Minnesotta hybrid density functional M06-2x at the 6-311+G(d,p) basis set.

Cell Based Studies—Cytotoxicity Studies of Rhein and Nanorhein: HEK-293 cells were seeded into 96 well plates and incubated for 24 h (at 37 °C 5% CO_2). Cells were then treated with varying concentrations of Rhein and Nanorhein (20–200 µM). After 24 hr incubation, MTT (0.5 mg mL^{-1}) was added to each well and kept at 37 °C for 4 hrs and finally the so formed formazan crystals were dissolved in DMSO and the OD was measured at 570 nm using a microplate reader.

Cell Culture: Cells were cultured in Dulbecco's modified Eagle medium (DMEM) supplemented with 1% penicillin streptomycin and

vs NC) and (*) $p < 0.05$ as compared with NRHD group (NC vs NRHD). c) Representative images of kidney sections stained with periodic acid–Schiff stain were scored for kidney injury. ➤ indicating Loss of brush border, ➡ indicates extended Bowmans space, and ➤ showing tubular dilation sites; scale bar: 1 mm. d) Representative images of H&E stained kidney sections are shown ➤-tubular casts; #-dilated tubules; scale bar: 1 mm.

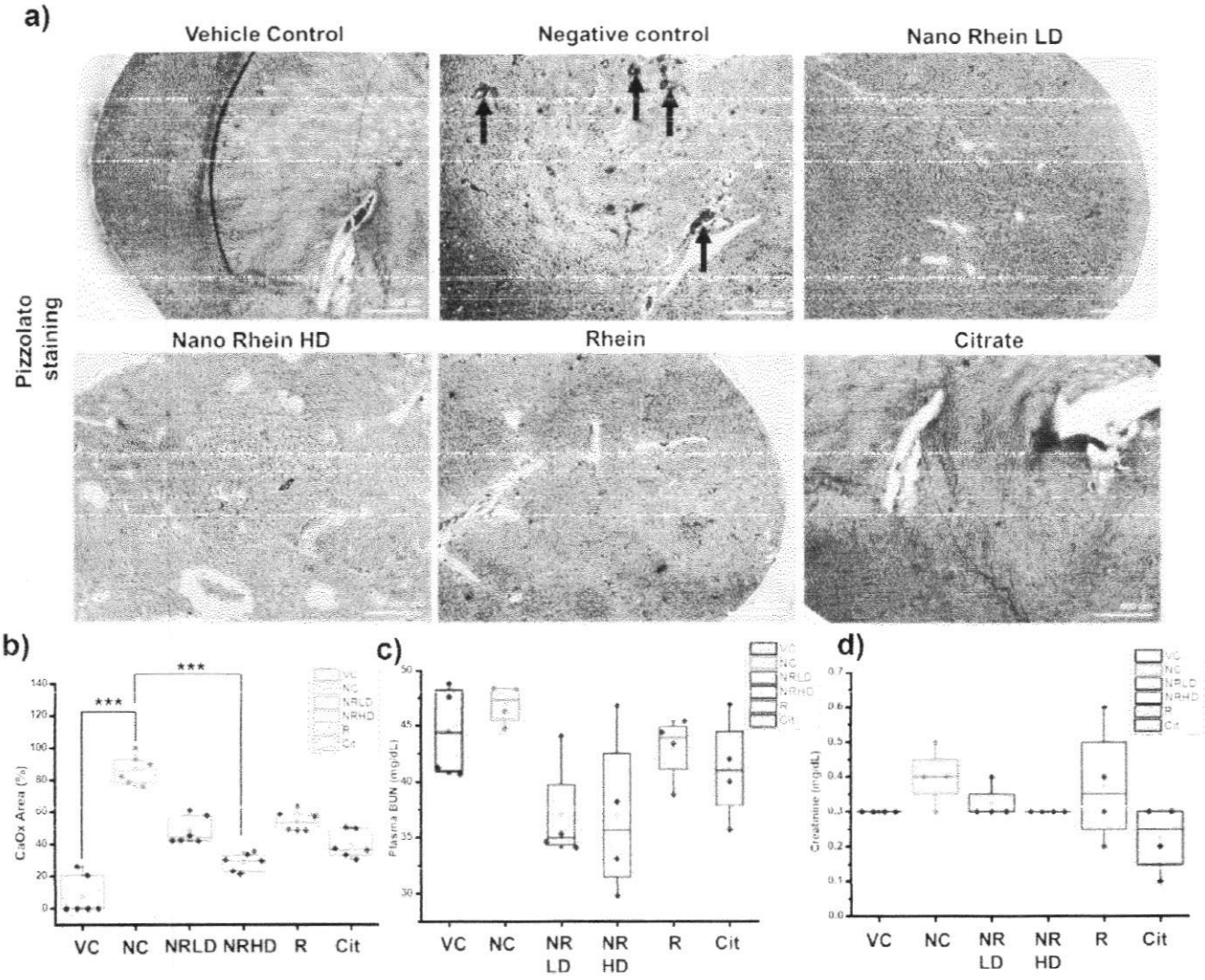

Figure 8. a) Representative images of kidney sections of mice were stained for CaOx deposition by Pizzolato staining and ➡ pointing to dark areas indicating CaOx.(scale bar. 500 μm) b) Quantification of CaOx by image]. Data are presented as mean ± SD (n=6). One-way ANOVA followed by a Tukey-Kramer multiple comparison test were performed. (***) $p < 0.001$ as compared with VC group (VC vs NC) and (***) $p < 0.001$ as compared with NRHD group (NC vs NRHD). c) Plasma blood urea nitrogen (BUN) was measured at day 7.(n=4) d) Creatinine was measured at day 7 (n=4). All Data are presented as mean ± SD (n = 4).

10% fetal bovine serum, under a 5% CO2 atmosphere at 37 °C until confluence was achieved. Confluent cells were harvested using 0.25% trypsin EDTA, which was subsequently neutralized with DMEM. The harvested cells were centrifuged, and the supernatant was discarded. The cells were then resuspended in DMEM to achieve the required concentration of cells ml^{-1}. Cell count was determined using a Petroff-Hausser cell counter. Cells were seeded on the respective culture plate/chamber slides by maintaining the cell number as per the assay requirements and incubated for 24 h.

Colocalization Studies: Confocal laser scanning microscopy (CLSM) was used to determine the subcellular localization of different preparations against HEK-293 cell lines. In brief, 5×10^5 cells were seeded on microscope coverslips in a six-well plate and cultured under 37 °C at 5% CO2 for 24 h. The medium was replaced by serum-free DMEM, and cells were incubated with different NR and R treatments at different time incubations. The cells were then preincubated with 400 nM MitoTracker Green for 30 minutes to visualize mitochondria. The cells were washed using cold PBS solution. Finally, the fluorescence intensity was determined by CLSM.

Metabolic Labeling of Cell Surface Glycans: Cells were then treated with the CaOx 500 μM or NR 50 μM/ CaOx 500 μM for another 24 hour incubation. Post-incubation, the cells were rinsed with PBS and treated with 100 μM of GlcNPhAlk and derived from a 50 mM stock solution in DMSO. The cells were then incubated for 60 h. Control cells were left untreated. Following incubation, all wells were washed thrice with HBSS buffer to remove excess compounds and unbound cells. Post-incubation, the cells were washed thrice with HBSS and prepared for SERS analysis.

Scanning Electron Microscopy (SEM) Studies: It was employed to prepare CaOx crystals using a Bis-Tris buffer (comprising 50 mm Bis-Tris, 150 mm NaCl, pH 6.2) containing final concentrations of 1 mm NaOx, 2 mm $CaCl_2$, and the specified concentration of the compound. Glass coverslips (12-mm round) were positioned at the base of 24-well plates. Initially, 20× stock solutions of $CaCl_2$ and inhibitor, and 10× NaOx were prepared in Bis-Tris buffer. The assay mixture was prepared in Eppendorf tubes by adding 800 μL of Bis-Tris buffer, followed by the addition of 50 μL $CaCl_2$ (20× concentration) and 50 μL of inhibitor (20× concentration), and vortexing. Subsequently, 100 μL NaOx (10× final concentra-

tion) was added, the assay mixture was vortexed and immediately transferred to the prepared 24-well plate. Two wells per sample were prepared with 400 µL per well. Samples were incubated at room temperature for the specified duration. Representative images were captured using a Leica DM 6000B microscope (Leica Microsystems) in brightfield mode before samples were rinsed once with double distilled water and air-dried at room temperature. Post-drying, samples were imaged again using bright-field microscopy to confirm minimal effects of the drying process on crystal morphology. After drying, glass coverslips were mounted on SEM stubs with silver paint and coated with a 6-nm layer of platinum/palladium using a CCU-010 Metal Sputter Coater (Safematic, Bad Ragaz, Switzerland). Samples were imaged using a Magellan 400 FEI SEM microscope (ThermoFisher Scientific) in the secondary electron mode using the TLD detector.

RNA Sequencing: Cells were cultured as described in the imaging assay and treated with a medium control (DMEM without any FBS), 500 µM CaOx, and 500 µM CaOx in a medium containing 50 µM rhein nanoparticles (NR) in the medium for 24 h. Total RNA was extracted using the RNeasy Mini Kit(74104) according to the manufacturer's instructions. The Qubit RNA BR Assay (Catalog number: Q10211) was used from Invitrogen to quantify RNA samples. For the assessment of RNA quality and integrity, the Agilent Tape Station system was used (Agilent, Cat# 5067-5576). Three wells per sample group were prepared, and the total RNA extracted from those three wells made them as the three technical replicates were pooled together for each biological replicate. Two biological replicates were used for the study. mRNA was purified, and the RNAseq library was prepared using the TrueSeq RNA kit (Illumina). Sequencing was performed on a Novaseq 6000 (Illumina). Reads were aligned to the reference human genome (hg38) using the STAR (2.4) tool. For the heatmap and hierarchical clustering of significantly different genes ($p \leq 0.05$, log2fold change ≥ 1). The heatmap was plotted using R software. differentially expressed genes with $p \leq 0.05$, log2fold change ≥ 0.5. Reactome pathway analysis of differentially expressed genes was analyzed in the – biological process functional database. The fragments per kilobase of the exon model per million reads mapped (FPKM) were used to compare the selected genes' expression levels, and two independent experiments were performed. RNA sequencing raw data can be made available to the corresponding author upon request.

Bioinformatics Analyses: Biological pathways enrichment analysis and the biological interpretation of the DEGs was achieved using the Reactome pathway database. Reactome analyses were performed to identify the functions of the DEGs. Only pathways and functional groups with p-values less than 0.05 were discussed. Volcano plots and functional enrichment plots were created using the SRplot web tool.

Animal Study: All animal experiments were performed in compliance with the regulations of the Institutional Animal Ethics Committee at the Kerala University (IAEC 2-KU-11/2024-ZOO-SRP (15)). Six groups of 42 male C57BL/6 mice of 6-8 weeks old were used for the study as per IAEC guidelines. Renal calcification was induced by administering glyoxylate (Gly) (75 mg $k^{-1}g$) intraperitonially (ip) for 7 days.[45,46] Nanorhein and rhein were administered simultaneously via intraperitoneal (i.p.) injection over the same period. Animals fed a normal diet and administered with PBS (i.p. 100 µL) served as the vehicle control group, while those receiving the Gly (i.p.) without treatment served as the negative control. Citrate, used as the standard treatment, was also administered intraperitoneally for 7 days. At the end of the treatment period, the animals were sacrificed, and their organs were collected for histopathological analysis. Blood and urine samples were also collected and subjected to hematological and biochemical parameter assessments.

Renal CaOx Crystals Detection: The kidney tissues were fixed, wax embedded, and sectioned. After staining with hematoxylin and eosin (HE), the CaOx crystals were observed under a polarized light optical microscope (Zeiss, Germany). Pizzolato staining was performed to visualize the CaOx crystals under an ordinary microscope. ImageJ software was used to quantify crystal deposition.

Assessment of Tubular Injury: Kidney sections were stained with periodic acid-Schiff (PAS) to evaluate tubular injury. Both the kidneys of the animals were evaluated, and ten fields were analyzed in the tissue samples of each animal. Signs of tubular injury such as tubular atrophy or dilation, cast formation, and brush edge loss were evaluated. Scoring was based on the percentage of damaged tubules as described in the previous study.[48]

Statistical Analysis: Data were presented as the mean ± SEM and the analysis was performed using GraphPad Prism 10. Multiple comparison between data sets were executed by 1-way ANOVA with post-hoc Tukey-Kramer test. P value less than 0.05 was considered as significant. The level of statistical significance was indicated as ***P<0.001, **P<0.01, *P<0.05.

Supporting Information

Supporting Information is available from the Wiley Online Library or from the author.

Acknowledgements

K.K.M. thanks CSIR and ICMR (project no. EM/IG/Dev.Res/2023-0001476), Government of India, for funding. V.P.M. thanks ICMR-DHR, Government of India, for the Young Scientist fellowship (R.12014/22/2021-HR/E-office:8114716); AcSIR Ph.D. student M.M thank UGC for research fellowship. K.K.M. and M.M thanks Dr. Arun A Rauf. Associate Professor &. Head. Department of. Biochemistry for his support in the in vivo study.

Conflict of Interest

The authors declare no conflict of interest.

Author Contributions

The manuscript was written through contributions of all authors. All authors have given approval to the final version of the manuscript.

Data Availability Statement

The data that support the findings of this study are available from the corresponding author upon reasonable request.

Keywords

calcium oxalate inhibitors, cassia fistula and transcriptomics, rhein, self-assembly

Received: August 31, 2025
Revised: September 10, 2025
Published online:

[1] A. Singh, S. Tandon, C. Tandon, *Mol. Biol. Rep.* **2021**, *48*, 887.
[2] M. R. Hayden, S. C. Tyagi, L. Kolb, J. R. Sowers, R. Khanna, *Cardiovasc. Diabetol.* **2005**, *4*, 1.
[3] W. Pan, W. Jie, H. Huang, *Med. Commun.* **2023**, *4*, e200.
[4] E. M. Worcester, F. L. Coe, *Semin. Nephrol.* **2008**, *28*, 120.
[5] Z. M. El-Zoghby, J. C. Lieske, R. N. Foley, E. J. Bergstralh, X. Li, *Clin. J. Am. Soc. Nephrol.* **2012**.
[6] S. R. Khan, *Urol. Res.* **2010**, *38*, 429.
[7] M. Ketteler, G. A. Block, P. Evenepoel, M. Fukagawa, C. A. Herzog, L. McCann, S. M. Moe, R. Shroff, M. A. Tonelli, N. D. Toussaint, M. G. Vervloet, M. B. Leonard, *Kidney Int.* **2017**, *92*, 26.